

Identification of NMF by choosing maximum-volume basis vectors

Qianqian Qi
Hangzhou Dianzi University, China
q.qi@hdu.edu.cn

Zhongming Chen
Hangzhou Dianzi University, China
zmchen@hdu.edu.cn

Peter G. M. van der Heijden
Utrecht University, the Netherlands and University of Southampton, UK
p.g.m.vanderheijden@uu.nl

Abstract

In nonnegative matrix factorization (NMF), minimum-volume-constrained NMF is a widely used framework for identifying the solution of NMF by making basis vectors as similar as possible. This typically induces sparsity in the coefficient matrix, with each row containing zero entries. Consequently, minimum-volume-constrained NMF may fail for highly mixed data, where such sparsity does not hold. Moreover, the estimated basis vectors in minimum-volume-constrained NMF may be difficult to interpret as they may be mixtures of the ground truth basis vectors. To address these limitations, in this paper we propose a new NMF framework, called maximum-volume-constrained NMF, which makes the basis vectors as distinct as possible. We further establish an identifiability theorem for maximum-volume-constrained NMF and provide an algorithm to estimate it. Experimental results demonstrate the effectiveness of the proposed method.

Keywords: Nonnegative matrix factorization, maximum-volume basis vectors, uniqueness, algorithm

1 Introduction

Nonnegative matrix factorization (NMF) has been a workhorse method used in many areas, such as blind hyperspectral unmixing, blind sound separation, image processing, text mining, and signal processing [1, 2, 3]. It aims to approximate a nonnegative matrix as a product of two lower-rank nonnegative matrices: given a matrix $\mathbf{X} \in \mathfrak{R}_+^{I \times J}$ and a dimensionality $K \leq \min\{I, J\}$, NMF searches for $\mathbf{M} \in \mathfrak{R}_+^{I \times K}$ and $\mathbf{H} \in \mathfrak{R}_+^{K \times J}$ such that \mathbf{MH} approximates \mathbf{X} as good as possible. Thus, NMF can be represented as

$$\begin{aligned} \mathbf{X} &\approx \mathbf{MH} \\ \text{subject to } \mathbf{M} &\in \mathfrak{R}_+^{I \times K}, \quad \mathbf{H} \in \mathfrak{R}_+^{K \times J}, \end{aligned} \tag{1}$$

where each column of \mathbf{M} represents a basis vector, and each column of \mathbf{H} contains the coefficients associated with the corresponding column (observation) of \mathbf{X} . In the noiseless setting, $\mathbf{X} = \mathbf{MH}$, which means $\mathbf{X}(:, j) \in \text{cone}(\mathbf{M})$. Given a matrix \mathbf{A} , $\text{cone}(\mathbf{A})$ is the convex cone generated by the columns of \mathbf{A} [2]. That is, $\text{cone}(\mathbf{A}) = \{\sum_j y_j \mathbf{A}(:, j) | y_j \geq 0\}$, where $\mathbf{A}(:, j)$ is the j th column of \mathbf{A} .

However, the solution to NMF (1) is not unique [2, 4, 5]. Specifically, if (\mathbf{M}, \mathbf{H}) is a solution of (1), $(\mathbf{MS}, \mathbf{S}^{-1}\mathbf{H})$ is also a solution of (1) for any invertible matrix $\mathbf{S} \in \mathfrak{R}^{K \times K}$, provided that both \mathbf{MS} and $\mathbf{S}^{-1}\mathbf{H}$ are nonnegative. Figure 1a illustrates this non-uniqueness for $I = K = 3$, and $J = 50$ in the noiseless setting. Figure 1a is obtained by assuming that the viewer is located in the nonnegative orthant, facing the origin, and observing

the unit-sum hyperplane $\mathbf{y}^T \mathbf{1} = 1$. In the figure, M_1, M_2, M_3 represent three estimated basis matrices of NMF of X . Three dashed triangles represent $\text{cone}(M_1)$, $\text{cone}(M_2)$, and $\text{cone}(M_3)$, respectively. As shown, blue dots (columns of X) lie within all three triangles, indicating that M_1, M_2 , and M_3 are all feasible basis matrices of NMF for X .

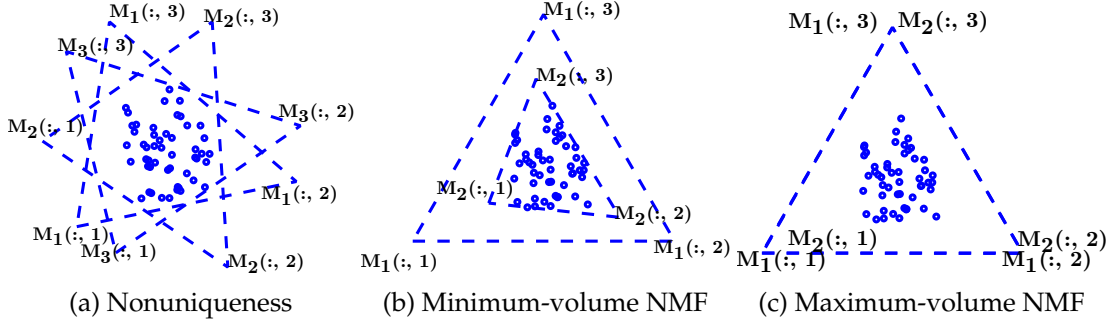


Figure 1: A graphical view of columns of the matrix X (blue dots) and $\text{cone}(M)$ (dashed triangle), sliced by the unit-sum hyperplane $\mathbf{y}^T \mathbf{1} = 1$: (a) nonuniqueness; (b) minimum-volume-constrained NMF; (c) maximum-volume-constrained NMF.

Minimum-volume-constrained NMF (MVC-NMF) is a widely used framework for identifying the basis matrix M and the coefficient matrix H . In the noiseless setting, MVC-NMF can be formulated as [6]:

$$\begin{aligned} \min \quad & \det(M^T M) \\ \text{subject to} \quad & X = MH, \quad M \in \mathfrak{R}_+^{I \times K}, \quad H \in \mathfrak{R}_+^{K \times J}, \\ & H^T \mathbf{1} = \mathbf{1}, \end{aligned} \quad (2)$$

where $\det(M^T M)$ denotes the determinant of $M^T M$. The $\det(M^T M)$ is used because $\sqrt{\det(M^T M)}/K!$ corresponds to the volume of the simplex formed by the origin and the columns of M [7, 8]. Given a matrix A , the convex hull of its columns, denoted by $\text{conv}(A)$, is the sets of all convex combination of its columns, i.e., $\text{conv}(A) = \{\sum_j y_j A(:, j) | y_j \geq 0, \sum_j y_j = 1\}$; if the columns $A(:, j)$, $j = 1, \dots, J$ are affine independent, then $\text{conv}(A)$ is a simplex. The constraint $H^T \mathbf{1} = \mathbf{1}$ in (2) can be replaced by $H \mathbf{1} = \mathbf{1}$ or $M^T \mathbf{1} = \mathbf{1}$ [7, 9].

Minimum-volume-constrained NMF is associated with sparsity in the coefficient matrix H . An artificial dataset is generated by using simulated matrices M and H , i.e., $X = MH$, where $I = 9$, $K = 3$, and $J = 50$. Figure 1b illustrates the sparsity of the coefficient matrix estimated by minimum-volume-constrained NMF. In the figure, M_1 denotes the ground truth basis matrix and M_2 denotes the estimated basis matrix by minimum-volume-constrained NMF. For visualization convenience, $M_1(:, 1)$, $M_1(:, 2)$, and $M_1(:, 3)$ are plotted as the vertices of an equilateral triangle; however, under the nonnegative orthant view, they do not necessarily form an equilateral triangle. Under the minimum-volume criterion (see the dashed triangle formed by M_2), there are data points, i.e., columns of X , on each boundary of the $\text{cone}(M_2)$. As a result, every row of the estimated coefficient matrix H_2 contains zero entries [10]. Furthermore, [6, 7, 9] showed that the solution to

(2) is unique when \mathbf{H} is satisfied with the so-called sufficiently scattered condition (SSC), which requires every row of \mathbf{H} to contain $K - 1$ zero entries. To summarize, the success of minimum-volume-constrained NMF relies on sparsity in the coefficient matrix \mathbf{H} .

While the minimum-volume assumption is appropriate in certain scenarios, it can be violated for highly mixed data, where the coefficient matrix \mathbf{H} does not contain zero entries in every row. As illustrated in Figure 1b, the basis matrix \mathbf{M}_2 estimated by minimum-volume-constrained NMF cannot recover the ground-truth basis matrix \mathbf{M}_1 . In addition, minimum-volume-constrained NMF minimizes $\det(\mathbf{M}^\top \mathbf{M})$, which makes the basis vectors as similar as possible. Consequently, the estimated basis vectors may be difficult to interpret. Moreover, the basis vectors estimated using minimum-volume-constrained NMF may remain mixtures of the ground truth basis vectors as shown in Figure 1b.

In this paper, we propose a new framework for NMF, coined maximum-volume-constrained NMF (MAV-NMF). In contrast to minimum-volume-constrained NMF, MAV-NMF maximizes the volume of \mathbf{M} . The basis vectors of this representation of NMF is more easily interpretable and unmixed and it is suitable for highly mixed data where the coefficient matrix does not contain zero entries in every row, as the estimated basis vectors are chosen to be as distinct as possible. We further establish an identifiability theorem for MAV-NMF and develop a strategy for estimating it. For the same artificial dataset as in Figure 1b, Figure 1c demonstrates the effectiveness of MAV-NMF using the algorithm that will be introduced in Section 3. As can be seen from the figure, the basis matrix \mathbf{M}_2 estimated by MAV-NMF coincides with the ground-truth basis matrix \mathbf{M}_1 . We note that the maximum-volume-constrained NMF proposed in this paper is fundamentally different from [11, 12]. Although the term maximum-volume in the context of NMF is used in [11, 12], but [11, 12] maximize the volume of \mathbf{H} , which is similar to minimizing the volume of \mathbf{M} .

The paper is built up as follows. Section 2 presents the MAV-NMF model and a condition guaranteeing its identifiability. In Section 3, we develop a strategy for estimating MAV-NMF. Numerical experiments to illustrate the performance of MAV-NMF are in Sections 4. Finally, in Section 5, we conclude.

2 Uniqueness theorem for maximum-volume-constrained NMF

In this section we propose maximum-volume-constrained nonnegative matrix factorization (MAV-NMF) and an uniqueness theorem for MAV-NMF. Most uniqueness theorems are established under the noiseless setting, which we assume in this section. Formally, the uniqueness or identifiability of the solution of nonnegative matrix factorization (NMF) is defined as follows.

Definition 1. [2, 13] *The NMF solution (\mathbf{M}, \mathbf{H}) of \mathbf{X} is said to be essentially unique if and only if any other NMF solution $(\tilde{\mathbf{M}}, \tilde{\mathbf{H}})$ can be expressed as*

$$\tilde{\mathbf{M}} = \mathbf{M}(\mathbf{\Gamma}\mathbf{\Sigma}) \text{ and } \tilde{\mathbf{H}} = (\mathbf{\Gamma}\mathbf{\Sigma})^{-1}\mathbf{H},$$

where $\mathbf{\Gamma}$ is a permutation matrix and $\mathbf{\Sigma}$ is a diagonal matrix with positive diagonal entries.

Here Γ allows for switching in the order of the columns of M and the rows of H , and Σ allows for the adjustment of the vector sizes.

In contrast to minimum-volume-constrained NMF (MVC-NMF) (2), MAV-NMF maximizes the determinant of $M^T M$ instead of minimizing it. MAV-NMF can be formulated as:

$$\begin{aligned} & \max \quad \det(M^T M) \\ & \text{subject to} \quad X = MH, \quad M \in \mathbb{R}_+^{I \times K}, \quad H \in \mathbb{R}_+^{K \times J}, \\ & \quad \quad \quad H^T \mathbf{1} = \mathbf{1}. \end{aligned} \quad (3)$$

As in MVC-NMF, the constraint $H^T \mathbf{1} = \mathbf{1}$ in (3) is replaced by $H \mathbf{1} = \mathbf{1}$ or $M^T \mathbf{1} = \mathbf{1}$.

Maximizing $\det(M^T M)$ is equivalent to minimizing $\det(HH^T)$. This can be seen by making use of a transformation matrix S . Suppose that (M, H) is a solution to the NMF model (1). Any solution of (1) can be written as $\tilde{M} = MS$ and $\tilde{H} = S^{-1}H$, where S is an invertible matrix. We have

$$\max \det(\tilde{M}^T \tilde{M}) \iff \max \det(S)^2 \iff \min \det(S)^{-2} \iff \min \det(\tilde{H} \tilde{H}^T). \quad (4)$$

Figure 2 gives a simple illustration of this relationship for $K = 3$. Figures 2a and 2c show $\text{cone}((MS)^T)$ and $\text{cone}(S^{-1}H)$ for MAV-NMF, respectively, while Figures 2b and 2d show $\text{cone}((MS)^T)$ and $\text{cone}(S^{-1}H)$ for MVC-NMF, respectively. As expected, $\text{cone}((MS)^T)$ is larger for MAV-NMF (Figure 2a) than for MVC-NMF (Figure 2b), whereas $\text{cone}(S^{-1}H)$ is smaller for MAV-NMF (Figure 2c) than for MVC-NMF (Figure 2d).

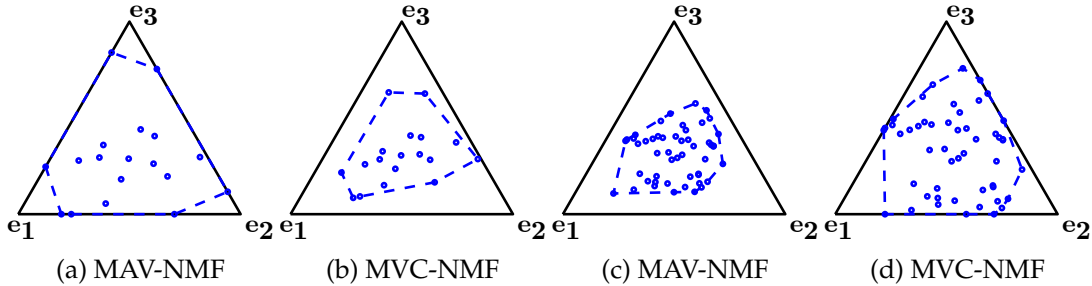


Figure 2: (a, b): A graphical representation of rows of the estimated basis matrix MS (blue dots), $\text{cone}(e_1, e_2, e_3)$ (solid triangle) with $e_1 = (1, 0, 0)^T$, $e_2 = (0, 1, 0)^T$, and $e_3 = (0, 0, 1)^T$, and $\text{cone}((MS)^T)$ (dashed polygon), sliced by the unit-sum hyperplane $\mathbf{y}^T \mathbf{1} = 1$; (c, d): A graphical representation of columns of the estimated coefficient matrix $S^{-1}H$ (blue dots), $\text{cone}(e_1, e_2, e_3)$ (solid triangle), and $\text{cone}(S^{-1}H)$ (dashed polygon), sliced by the unit-sum hyperplane $\mathbf{y}^T \mathbf{1} = 1$.

A sufficient condition of the uniqueness of the solution of MVC-NMF relies on the sufficiently scattered condition (SSC) in the coefficient matrix H [6, 7, 9]. In contrast, for MAV-NMF, we impose the SSC on the transpose of the basis matrix, M^T . M^T is said to satisfy SSC if [2, 6, 7, 9, 13]:

(1) SSC1: $\mathbb{C} \subseteq \text{cone}(M^T)$, where $\text{cone}(M^T) = \{\sum_i y_i M(i, :)^T | y_i \geq 0\}$, with $M(i, :) \in \mathbb{R}_+^{1 \times K}$ denoting the i th row of M ; moreover, $\mathbb{C} = \{\mathbf{y} \in \mathbb{R}_+^K | \mathbf{1}^T \mathbf{y} \geq \sqrt{K-1} \|\mathbf{y}\|_2\}$, which is

a second-order cone;

(2) SSC2: $\text{cone}^*(\mathbf{M}^T) \cap \text{bd}\mathbb{C}^* = \{\alpha \mathbf{e}_k | \alpha \geq 0, k = 1, \dots, K\}$, where the dual cone of \mathbf{M}^T is $\text{cone}^*(\mathbf{M}^T) = \{\mathbf{y} | \mathbf{M}\mathbf{y} \geq 0\}$, the dual cone of \mathbb{C} is $\mathbb{C}^* = \{\mathbf{y} \in \mathbb{R}^K | \mathbf{1}^T \mathbf{y} \geq \|\mathbf{y}\|_2\}$, and $\text{bd}\mathbb{C}^*$ is the boundary of \mathbb{C}^* .

Now, we present an identifiability theorem for the solution of MVA-NMF, which relies on the SSC in the transpose of the basis matrix: \mathbf{M}^T .

Theorem 1. *Assume that (1) $\text{rank}(\mathbf{M}) = \text{rank}(\mathbf{H}) = K$, (2) \mathbf{M}^T satisfies SSC. Then MAV-NMF uniquely identifies $\tilde{\mathbf{M}}$ and $\tilde{\mathbf{H}}$ up to permutation. That is, any optimal solution $(\mathbf{M}_\#, \mathbf{H}_\#)$ of MAV-NMF (3) can be expressed as:*

$$\mathbf{M}_\# = \tilde{\mathbf{M}}\mathbf{\Gamma} \text{ and } \mathbf{H}_\# = \mathbf{\Gamma}^{-1}\tilde{\mathbf{H}}$$

where $\mathbf{\Gamma}$ is a permutation matrix.

The proof of Theorem 1 follows arguments similar to those developed for MVC-NMF in [6, 7, 9] and is provided in the supplementary materials.

In MAV-NMF, the SSC is imposed on the transpose \mathbf{M}^T of the basis matrix rather than on the coefficient matrix \mathbf{H} , as in MVC-NMF. The SSC is closely related to sparsity: if \mathbf{M}^T satisfies SSC, each column of \mathbf{M} contains at least $K - 1$ zero entries [2, 13]. Consequently, MAV-NMF promotes sparsity in the basis matrix \mathbf{M} instead of in the coefficient matrix \mathbf{H} , which can be advantageous for highly mixed data and leads to basis vectors that are more easily interpretable than those in MVC-NMF. In Figure 2a, $(\mathbf{M}\mathbf{S})^T$ satisfies SSC, and thus the solution of MAV-NMF is unique.

3 A simple approach for solving maximum-volume-constrained NMF

In general, $\mathbf{X} - \mathbf{M}\mathbf{H} \neq \mathbf{0}$. The objective function of maximum-volume-constrained NMF (MAV-NMF) can be formulated as

$$\begin{aligned} \min \quad & \|\mathbf{X} - \mathbf{M}\mathbf{H}\|_F^2 - \lambda \log \det(\mathbf{M}^T \mathbf{M} + \delta \mathbf{I}) \\ \text{subject to} \quad & \mathbf{M} \in \mathbb{R}_+^{I \times K}, \quad \mathbf{H} \in \mathbb{R}_+^{K \times J}, \quad \mathbf{H}^T \mathbf{1} = \mathbf{1}, \end{aligned} \quad (5)$$

where $\|\mathbf{X} - \mathbf{M}\mathbf{H}\|_F^2$ is the data-fitting term and $\log \det(\mathbf{M}^T \mathbf{M} + \delta \mathbf{I})$ is the volume regularization term, with $\delta > 0$ and $\lambda > 0$ [8, 14]. For a given matrix $\mathbf{A} \in \mathbb{R}^{I \times J}$, the Frobenius norm $\|\mathbf{A}\|_F^2$ is defined as $\|\mathbf{A}\|_F^2 = \sqrt{\sum_i \sum_j \mathbf{A}(i, j)^2}$. The parameter λ controls the trade-off between the data-fitting term and the volume regularizer. The main difference between MAV-NMF and the minimum-volume-constrained NMF (MVC-NMF) in [14] lies in the sign before the volume regularization term: a negative sign in (5) favors larger values of $\log \det(\mathbf{M}^T \mathbf{M} + \delta \mathbf{I})$. The constraint $\mathbf{H}^T \mathbf{1} = \mathbf{1}$ in (5) can be replaced by $\mathbf{H}\mathbf{1} = \mathbf{1}$ or $\mathbf{M}^T \mathbf{1} = \mathbf{1}$. Note that maximizing $\log \det(\mathbf{M}^T \mathbf{M})$ avoids $\mathbf{M}^T \mathbf{M}$ to be singular. Here we

use $\log\det(\mathbf{M}^T \mathbf{M} + \delta \mathbf{I})$ instead of $\log\det(\mathbf{M}^T \mathbf{M})$ because we will replace the negative volume term with a positive term, see (6).

The objective function in (5) is non-convex. As in [2, 11, 14, 15, 16], we adopt an alternating optimization scheme over \mathbf{M} and \mathbf{H} : iteratively updating \mathbf{M} for fixed \mathbf{H} and updating \mathbf{H} for fixed \mathbf{M} . The main difficulty in solving (5) with respect to \mathbf{M} lies in the term $-\lambda \log\det(\mathbf{M}^T \mathbf{M} + \delta \mathbf{I})$ [11, 12]. Since the $\log\det(\mathbf{Q})$ is concave, the first-order Taylor expansion is a majorizer of $\log\det(\mathbf{Q})$ on the set of positive definite matrices \mathbf{Q} and it is then possible to update \mathbf{M} by minimizing the obtained majorizer as in [8, 14]. However, since $-\log\det(\mathbf{Q})$ is convex, it prevents us from using this strategy.

As discussed in the previous section (see (4)), in the noiseless setting, maximizing $\det(\mathbf{M}^T \mathbf{M})$ is equivalent to minimizing $\det(\mathbf{H}\mathbf{H}^T)$. Motivated by this equivalence, we reformulate (5) as the following optimization problem:

$$\begin{aligned} \min \quad & \|\mathbf{X} - \mathbf{M}\mathbf{H}\|_F^2 + \lambda \log\det(\mathbf{H}\mathbf{H}^T + \delta \mathbf{I}) \\ \text{subject to} \quad & \mathbf{M} \in \mathfrak{R}_+^{I \times K}, \quad \mathbf{H} \in \mathfrak{R}_+^{K \times J}, \quad \mathbf{H}^T \mathbf{1} = \mathbf{1}. \end{aligned} \quad (6)$$

In other words, by replacing $-\lambda \log\det(\mathbf{M}^T \mathbf{M} + \delta \mathbf{I})$ in (5) with $\lambda \log\det(\mathbf{H}\mathbf{H}^T + \delta \mathbf{I})$ in (6), the negative log-determinant term of $\mathbf{M}^T \mathbf{M} + \delta \mathbf{I}$ is effectively removed from the optimization problem. As in (5), the constraint $\mathbf{H}^T \mathbf{1} = \mathbf{1}$ in (6) can be replaced by $\mathbf{H}\mathbf{1} = \mathbf{1}$ or $\mathbf{M}^T \mathbf{1} = \mathbf{1}$.

Problem (6) can be solved by considering

$$\begin{aligned} \min_{\mathbf{M}, \mathbf{H}} \quad & \|\mathbf{X} - \mathbf{M}\mathbf{H}\|_F^2 + \lambda \log\det(\mathbf{M}^T \mathbf{M} + \delta \mathbf{I}) \\ \text{subject to} \quad & \mathbf{M} \in \mathfrak{R}_+^{I \times K}, \quad \mathbf{H} \in \mathfrak{R}_+^{K \times J}, \quad \mathbf{M}\mathbf{1} = \mathbf{1}, \end{aligned} \quad (7)$$

making use of $\mathbf{X}^T = \mathbf{H}^T \mathbf{M}^T$. Similar to how the constraint $\mathbf{M}\mathbf{1} = \mathbf{1}$ in (7) replaces $\mathbf{H}^T \mathbf{1} = \mathbf{1}$ in (6), the alternative constraints $\mathbf{H}\mathbf{1} = \mathbf{1}$ and $\mathbf{M}^T \mathbf{1} = \mathbf{1}$ in (6) correspond to $\mathbf{M}^T \mathbf{1} = \mathbf{1}$ and $\mathbf{H}\mathbf{1} = \mathbf{1}$ in (7), respectively. In this paper, we use the algorithm in [14] which solved $\min \|\mathbf{X} - \mathbf{M}\mathbf{H}\|_F^2 + \lambda \log\det(\mathbf{M}^T \mathbf{M} + \delta \mathbf{I})$. We call the algorithm APFGM-LOGDET, short for alternative projected fast gradient methods for logdet regularized objective function. The algorithm from [14] is provided in Algorithm 1 and briefly outlined here. Given \mathbf{M} , the objective for \mathbf{H} is

$$\min_{\mathbf{H} \geq 0} \|\mathbf{X} - \mathbf{M}\mathbf{H}\|_F^2. \quad (8)$$

One updates \mathbf{H} using a projected fast gradient method (PFGM) [2, 14], which can incorporate constraints such as nonnegativity, column-sum-to-1, or row-sum-to-1. Given \mathbf{H} , the objective for \mathbf{M} is $\min_{\mathbf{M} \geq 0, \mathbf{M}\mathbf{1}=\mathbf{1}} \|\mathbf{X} - \mathbf{M}\mathbf{H}\|_F^2 + \lambda \log\det(\mathbf{M}^T \mathbf{M} + \delta \mathbf{I})$. One updates \mathbf{M} by applying PFGM to its strongly convex upper approximation:

$$\min_{\mathbf{M} \in \mathfrak{R}_+^{I \times K}, \mathbf{M}\mathbf{1}=\mathbf{1}} 2 \sum_{i=1}^I \left(\frac{1}{2} \mathbf{M}(i, :) \mathbf{A} \mathbf{M}(i, :)^T - \mathbf{C}(i, :) \mathbf{M}(i, :)^T \right), \quad (9)$$

where $\mathbf{A} = \mathbf{H}\mathbf{H}^T + \lambda(\mathbf{M}_0^T \mathbf{M}_0 + \delta \mathbf{I})^{-1}$ and $\mathbf{C} = \mathbf{X}\mathbf{H}^T$.

Algorithm 1: APFGM-LOGDET (7).

Input: \mathbf{X} , K , λ' , and *maxiter*.

Output: $\mathbf{M} \geq 0$ and $\mathbf{H} \geq 0$.

Generate initial matrices $\mathbf{M}^{(0)} \geq 0$ and $\mathbf{H}^{(0)} \geq 0$. Let $\lambda = \lambda' \frac{\|\mathbf{X} - \mathbf{M}^{(0)} \mathbf{H}^{(0)}\|_F^2}{|\log \det(\mathbf{M}^T \mathbf{M} + \delta \mathbf{I})|}$.

for $t = 1, 2, \dots, \textit{maxiter}$ **do**

 PFGM is performed on (8) to update \mathbf{H}

 PFGM is performed on (9) to update \mathbf{M}

4 Numerical experiments

In this section, we evaluate the performance of maximum-volume-constrained NMF (MAV-NMF) on two artificial grain-size distribution datasets from [17] in sedimentary geology, three artificial datasets simulated by us, a real-world human face images dataset from image processing, and a real-world time-allocation dataset from social science, where the three artificial datasets simulated by us are provided in the supplementary materials for saving space. For the artificial datasets, the ground truth basis and coefficient matrices are known, whereas for the real-world datasets, the ground truth is unknown. We compare MAV-NMF with minimum-volume-constrained NMF (MVC-NMF). All methods are implemented in MATLAB R2024b, and the code is available at <https://github.com/qianqianqi28/MAV-NMF>.

4.1 Sedimentary geology: Grain-size distributions dataset

NMF can be used to unmix grain-size distribution (GSD) datasets, providing insights into sediment provenance, transport, and sedimentation processes [17, 18, 19, 20, 21, 22, 23, 24]. We use two artificial datasets from [17]. Figure 3a shows the four basis vectors, each with 28 values, used in [17] to generate the two artificial datasets. These basis vectors were derived from grain-size data of surface sediments in the South Yellow Sea [19].

For Test Dataset 1 with $I = 28$ and $J = 200$, the coefficient matrix of size 4×200 has a minimum value of 0.0003 and a maximum value of 0.8006; therefore, it contains no zero entries. Test Dataset 2 with $I = 25$ and $J = 200$ represents more highly mixed data generated from bases 1-3, with coefficients ranging from 0.0506 to 0.7939. The last three entries of bases 1-3 are zero; hence, they have been omitted in Test Dataset 2.

We apply MVC-NMF and MAV-NMF to Test Datasets 1 and 2. As shown in Figure 3b, MAV-NMF recovers basis vectors that are more consistent with the ground truth bases than those obtained by MVC-NMF. In particular, for MVC-NMF, the estimated basis 1 exhibits two peaks: one coincides with the peak of the ground truth basis 1, while the other lies between those of bases 3 and 4. A closer inspection of the estimated basis vectors shows

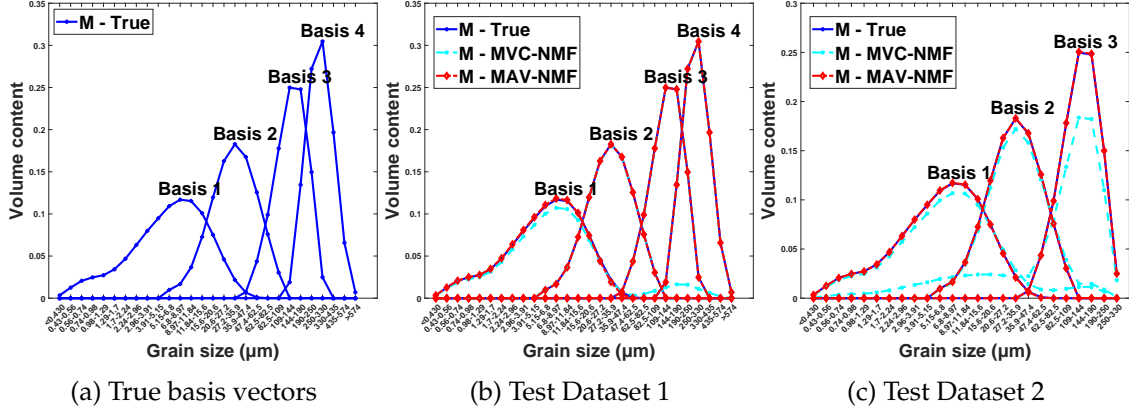


Figure 3: Artificial grain-size distributions (GSDs) datasets from [17] (a) The four ground truth basis vectors used from [17], which were from the calculated EMs from the grain-size data of the surface sediment in the South Yellow Sea by [19]; (b) Test Dataset 1; (c) Test Dataset 2.

Table 1: Artificial grain size distributions datasets; $\log \det(M^T M + \delta I)$

Methods	Test Dataset 1	Test Dataset 2
MVC-NMF	-5.7100	-4.9230
MAV-NMF	-5.6270	-4.4340

that

$$\begin{aligned}
 \text{estimated basis 1 by MVC-NMF} &\approx 0.9173 \times \text{ground truth basis 1} \\
 &\quad + 0.0490 \times \text{ground truth basis 3} \\
 &\quad + 0.0320 \times \text{ground truth basis 4}.
 \end{aligned}$$

Therefore, the estimated basis 1 produced by MVC-NMF does not correspond to a single ground truth basis but remains a mixture of multiple ground truth basis vectors. Moreover, the coefficient matrix estimated by MVC-NMF contains zero entries, which contradicts the true setting in which no coefficients are zero. These effects are even more pronounced for Test Dataset 2, which is more highly mixed than Test Dataset 1.

Table 1 reports $\log \det(M^T M + \delta I)$, from which we observe that the volume obtained by MAV-NMF is larger than that obtained by MVC-NMF.

The three artificial datasets simulated by us in the supplementary materials has similar results, namely MAV-NMF produces better results than MVC-NMF for highly mixed data.

4.2 Image processing: Human face images dataset

We apply MVC-NMF and MAV-NMF to the CBCL face dataset of $J = 2,429$ face images, each consisting of $I = 19 \times 19$ pixels, i.e., $\mathbf{X} \in \mathbb{R}_+^{361 \times 2429}$ [1, 2]. For this dataset, in (7) we use the constraint $\mathbf{H}\mathbf{1} = \mathbf{1}$ instead of the constraint $\mathbf{M}\mathbf{1} = \mathbf{1}$. Following [1, 2], we set the dimensionality to $K = 49$. Figure 4a and Figure 4b present the basis matrices \mathbf{M} estimated by MVC-NMF and MAV-NMF, respectively. Each estimated basis matrix $\mathbf{M} \in \mathbb{R}_+^{361 \times 49}$ is

reshaped into 49 individual images and displayed in a 7×7 grid, where positive values are displayed as black pixels.

We observe that the basis obtained by MAV-NMF is substantially sparser than those produced by MVC-NMF, which is consistent with the theoretical analysis in Section 2. Moreover, the 49 basis images estimated by MAV-NMF contain multiple distinct versions of eyes, noses, and other facial parts, aligning better with intuitive facial parts. Table 2 reports $\log \det(M^T M + \delta I)$, showing that MAV-NMF yields a larger volume than MVC-NMF.

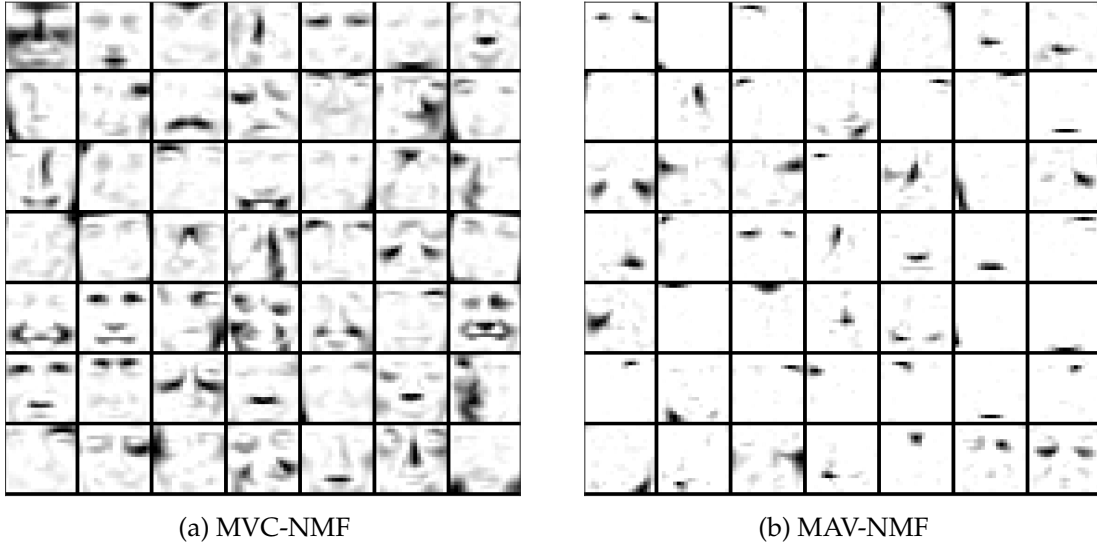


Figure 4: CBCL face data set: (a) MVC-NMF; (b) MAV-NMF.

Table 2: Real-world CBCL dataset; $\log \det(M^T M + \delta I)$

Methods	CBCL
MVC-NMF	-107.7660
MAV-NMF	-90.4210

4.3 Social science: Time allocation dataset

We analyze a time-allocation dataset, where $I = 18$ corresponds to 18 activities (e.g., paid work, domestic work, and caring for household members) and $J = 30$ represents groups cross-classified by gender (male and female), age (12–24, 25–34, 35–49, 50–64, and > 65), and survey year (1975, 1980, and 1985) [25, 26]. The dataset is available in [25, 26] as well as in the supplementary materials. The columns of the dataset have nearly identical sums. Before applying MVC-NMF and MAV-NMF, we normalize the dataset so that the sum of each column equals 1.

Table 3 reports the results of MVC-NMF and MAV-NMF for $K = 3$, where M3580 denotes males aged 35–49 in the 1980 survey and F5075 denotes females aged 50–64 in the 1975 survey, and similarly for the other group labels. In addition, the table includes

the results of $K = 1$ as reference, where \mathbf{M} is the average of the row sums of the time-allocation dataset provided in the supplementary materials and \mathbf{H} is a matrix of ones. From the table, we observe that MAV-NMF tends to produce a sparser basis matrix \mathbf{M} and a less sparse coefficient matrix \mathbf{H} compared with MVC-NMF. This sparsity in the basis matrix improves interpretability: by comparing \mathbf{M} for $K = 1$, dimension 1 is mainly associated with domestic work and caring for household members, dimension 2 with paid work, and dimension 3 with education. Table 4 reports $\log \det(\mathbf{M}^\top \mathbf{M} + \delta \mathbf{I})$, again showing that MAV-NMF yields a larger volume than MVC-NMF.

Table 3: Time allocation dataset for dimensionality $K = 3$ using MVC-NMF and MAV-NMF, where M3580 denotes males aged 35-49 in the 1980 survey and F5075 denotes females aged 50-64 in the 1975 survey, and similarly for the other group labels.

Model	/	MVC-NMF			MAV-NMF		
		$k = 1$	$k = 1$	$k = 2$	$k = 3$	$k = 1$	$k = 2$
\mathbf{M}							
paidwork	0.0803	0.0000	0.2180	0.0630	0.0000	0.2499	0.0000
dom.work	0.0779	0.1471	0.0171	0.0042	0.1460	0.0000	0.0000
caring	0.0167	0.0241	0.0162	0.0000	0.0237	0.0133	0.0000
shopping	0.0253	0.0360	0.0165	0.0131	0.0360	0.0137	0.0104
per.need	0.0347	0.0371	0.0318	0.0332	0.0371	0.0310	0.0336
eating	0.0623	0.0642	0.0675	0.0496	0.0642	0.0683	0.0401
sleeping	0.3581	0.3635	0.3348	0.3811	0.3637	0.3301	0.4034
educat.	0.0335	0.0000	0.0000	0.1694	0.0000	0.0000	0.2571
particip	0.0146	0.0156	0.0163	0.0094	0.0156	0.0166	0.0056
soc.cont	0.0656	0.0776	0.0587	0.0473	0.0776	0.0561	0.0404
goingout	0.0297	0.0220	0.0321	0.0444	0.0220	0.0334	0.0515
sports	0.0363	0.0426	0.0230	0.0417	0.0427	0.0199	0.0505
gardening	0.0194	0.0200	0.0258	0.0083	0.0200	0.0267	0.0000
outside	0.0061	0.0057	0.0075	0.0049	0.0057	0.0079	0.0034
tv-radio	0.0779	0.0773	0.0789	0.0777	0.0775	0.0793	0.0758
reading	0.0359	0.0419	0.0344	0.0236	0.0420	0.0335	0.0170
relaxing	0.0070	0.0076	0.0058	0.0074	0.0076	0.0055	0.0081
other	0.0188	0.0198	0.0154	0.0216	0.0198	0.0147	0.0245
\mathbf{H}^\top							
M1275	1.0000	0.0000	0.1623	0.8377	0.0805	0.3662	0.5534
M1280	1.0000	0.0561	0.1005	0.8434	0.1304	0.3137	0.5559
M1285	1.0000	0.0480	0.0593	0.8927	0.1205	0.2913	0.5882
M2575	1.0000	0.0000	0.9542	0.0458	0.1232	0.8384	0.0384
M2580	1.0000	0.0349	0.8541	0.1109	0.1504	0.7691	0.0805
M2585	1.0000	0.0805	0.8192	0.1003	0.1908	0.7362	0.0730
M3575	1.0000	0.0897	0.8594	0.0509	0.2037	0.7582	0.0381
M3580	1.0000	0.0682	0.8899	0.0419	0.1844	0.7820	0.0336
M3585	1.0000	0.0492	0.9256	0.0252	0.1678	0.8084	0.0238
M5075	1.0000	0.1542	0.7876	0.0582	0.2612	0.6984	0.0404
M5080	1.0000	0.2721	0.6337	0.0943	0.3624	0.5751	0.0625
M5085	1.0000	0.3407	0.5709	0.0885	0.4225	0.5196	0.0579
M6575	1.0000	0.6952	0.1508	0.1539	0.7309	0.1740	0.0951
M6580	1.0000	0.6956	0.0989	0.2055	0.7299	0.1433	0.1268
M6585	1.0000	0.7017	0.1085	0.1897	0.7351	0.1475	0.1174
F1275	1.0000	0.2410	0.1168	0.6422	0.3004	0.2738	0.4258
F1280	1.0000	0.2076	0.0588	0.7336	0.2662	0.2481	0.4857
F1285	1.0000	0.1886	0.0000	0.8114	0.2463	0.2173	0.5363
F2575	1.0000	0.8230	0.1770	0.0000	0.8431	0.1547	0.0022
F2580	1.0000	0.8126	0.1845	0.0028	0.8291	0.1603	0.0105
F2585	1.0000	0.6889	0.2964	0.0147	0.7214	0.2602	0.0184
F3575	1.0000	0.9102	0.0898	0.0000	0.9192	0.0808	0.0000
F3580	1.0000	0.8945	0.1055	0.0000	0.9055	0.0945	0.0000
F3585	1.0000	0.8632	0.1368	0.0000	0.8785	0.1215	0.0000
F5075	1.0000	0.9690	0.0310	0.0000	0.9699	0.0301	0.0000
F5080	1.0000	0.9672	0.0328	0.0000	0.9686	0.0314	0.0000
F5085	1.0000	0.9192	0.0806	0.0002	0.9259	0.0725	0.0016
F6575	1.0000	0.9501	0.0049	0.0451	0.9534	0.0190	0.0275
F6580	1.0000	0.9683	0.0000	0.0317	0.9693	0.0096	0.0211
F6585	1.0000	0.9342	0.0088	0.0570	0.9391	0.0259	0.0350

Table 4: Real-world time allocation dataset; $\log\det(\mathbf{M}^T \mathbf{M} + \delta \mathbf{I})$

Methods	Time allocation
MVC-NMF	-4.6060
MAV-NMF	-4.2750

5 Conclusion

This paper introduces a new NMF framework, termed maximum-volume-constrained NMF (MAV-NMF), which encourages the learned basis vectors to be as distinct as possible. In contrast to minimum-volume-constrained NMF (MVC-NMF), MAV-NMF is particularly suitable for highly mixed data, where the rows of the coefficient matrix do not contain zero entries, and it tends to yield more interpretable and unmixed basis vectors. We provide a sufficient condition, related to the sufficiently scattered condition, under which the solution of MAV-NMF is unique. To estimate MAV-NMF, we exploit an equivalent transformation that replaces the negative determinant regularization on the basis matrix with the positive one on the coefficient matrix. Finally, we demonstrate the performance of MAV-NMF on two artificial sedimentary geology datasets, three additional datasets generated by us, a human face images dataset, and a social science time-allocation dataset.

Acknowledgments

Zhongming Chen is partially supported by Natural Science Foundation of Zhejiang Province (No. LY22A010012) and Natural Science Foundation of Xinjiang Uygur Autonomous Region (No. 2024D01A09).

Competing Interests

No potential competing interest was reported by the authors.

References

- [1] Daniel D. Lee and H. Sebastian Seung. Learning the parts of objects by non-negative matrix factorization. *Nature*, 401(6755):788–791, 1999.
- [2] Nicolas Gillis. *Nonnegative Matrix Factorization*. Society for Industrial and Applied Mathematics, Philadelphia, PA, 2020.
- [3] Farid Saberi-Movahed, Kamal Berahmand, Razieh Sheikhpour, Yuefeng Li, Shirui Pan, and Mahdi Jalili. Nonnegative matrix factorization in dimensionality reduction: A survey. *ACM Computing Surveys*, 58(5), 2025.
- [4] Xiao Fu, Kejun Huang, Nicholas D. Sidiropoulos, and Wing-Kin Ma. Nonnegative matrix factorization for signal and data analytics: Identifiability, algorithms, and applications. *IEEE Signal Processing Magazine*, 36(2):59–80, 2019.
- [5] Maryam Abdolali, Giovanni Barbarino, and Nicolas Gillis. Dual simplex volume maximization for simplex-structured matrix factorization. *SIAM Journal on Imaging Sciences*, 17(4):2362–2391, 2024.
- [6] Xiao Fu, Wing-Kin Ma, Kejun Huang, and Nicholas D. Sidiropoulos. Blind separation of quasi-stationary sources: Exploiting convex geometry in covariance domain. *IEEE Transactions on Signal Processing*, 63(9):2306–2320, 2015.
- [7] Valentin Leplat, Nicolas Gillis, and Andersen M.S. Ang. Blind audio source separation with minimum-volume beta-divergence NMF. *IEEE Transactions on Signal Processing*, 68:3400–3410, 2020.
- [8] Xiao Fu, Kejun Huang, Bo Yang, Wing-Kin Ma, and Nicholas D. Sidiropoulos. Robust volume minimization-based matrix factorization for remote sensing and document clustering. *IEEE Transactions on Signal Processing*, 64(23):6254–6268, 2016.
- [9] Xiao Fu, Kejun Huang, and Nicholas D. Sidiropoulos. On identifiability of nonnegative matrix factorization. *IEEE Signal Processing Letters*, 25(3):328–332, 2018.
- [10] Guoxu Zhou, Shengli Xie, Zuyuan Yang, Jun-Mei Yang, and Zhaoshui He. Minimum-volume-constrained nonnegative matrix factorization: Enhanced ability of learning parts. *IEEE Transactions on Neural Networks*, 22(10):1626–1637, 2011.
- [11] Gokcan Tatli and Alper T. Erdogan. Polytopic matrix factorization: Determinant maximization based criterion and identifiability. *IEEE Transactions on Signal Processing*, 69:5431–5447, 2021.
- [12] Olivier Vu Thanh and Nicolas Gillis. Maximum-volume nonnegative matrix factorization. *arXiv preprint arXiv:2602.04795*, 2026.

- [13] Kejun Huang, Nicholas D. Sidiropoulos, and Ananthram Swami. Non-negative matrix factorization revisited: Uniqueness and algorithm for symmetric decomposition. *IEEE Transactions on Signal Processing*, 62(1):211–224, 2014.
- [14] Valentin Leplat, Andersen M.S. Ang, and Nicolas Gillis. Minimum-volume rank-deficient nonnegative matrix factorizations. In *ICASSP 2019 - 2019 IEEE International Conference on Acoustics, Speech and Signal Processing (ICASSP)*, pages 3402–3406, 2019.
- [15] Andersen Man Shun Ang and Nicolas Gillis. Algorithms and comparisons of non-negative matrix factorizations with volume regularization for hyperspectral unmixing. *IEEE Journal of Selected Topics in Applied Earth Observations and Remote Sensing*, 12(12):4843–4853, 2019.
- [16] Andersen Ang, Waqas Bin Hamed, and Hans De Sterck. Sum-of-norms regularized nonnegative matrix factorization. *Neural Computation*, 38(2):228–255, 2026.
- [17] Xiaodong Zhang, Hongmin Wang, Shumei Xu, and Zuosheng Yang. A basic end-member model algorithm for grain-size data of marine sediments. *Estuarine, Coastal and Shelf Science*, 236:106656, 2020.
- [18] Greig A. Paterson and David Heslop. New methods for unmixing sediment grain size data. *Geochemistry, Geophysics, Geosystems*, 16(12):4494–4506, 2015.
- [19] Xiaodong Zhang, Yang Ji, Zuosheng Yang, Zhongbo Wang, Dongsheng Liu, and Peimeng Jia. End member inversion of surface sediment grain size in the south yellow sea and its implications for dynamic sedimentary environments. *Science China Earth Sciences*, 59(2):258–267, 2016.
- [20] J.A. Van Hateren, M.A. Prins, and R.T. Van Balen. On the genetically meaningful decomposition of grain-size distributions: A comparison of different end-member modelling algorithms. *Sedimentary Geology*, 375:49–71, 2018.
- [21] Yuming Liu, Ting Wang, Bo Liu, Yili Long, Xingxing Liu, and Youbin Sun. Universal decomposition model: An efficient technique for palaeoenvironmental reconstruction from grain-size distributions. *Sedimentology*, 70(7):2127–2149, 2023.
- [22] Damian Moskalewicz and Christian Winter. Identification of sandy nourished sediments using end-member analysis (emmageo) applied to particle shapes distributions, sylt island, north sea. *Marine Geology*, 467:107201, 2024.
- [23] Zhanyi Lin, Qiuchi Wan, Fan Zhang, Jing Zhong, Zhongle Zhou, and Kunshan Bao. Using end-member model algorithm to infer sedimentary processes from mangrove sediment grain-size in guangdong, south china. *Regional Studies in Marine Science*, 83:104069, 2025.
- [24] Adhra Renny, Masud Kawsar, M.C. Manoj, Srinivas Bikkina, Binita Phartiyal, P. John Kurian, Ravi Mishra, and Biswajeet Thakur. Decoding the sedimentary responses to

the monsoon seasonality and ocean circulation in the southeast arabian sea during the last 50 ka. *Palaeogeography, Palaeoclimatology, Palaeoecology*, 681:113384, 2026.

- [25] Ab Mooijaart, Peter G.M. Van der Heijden, and L.Andries Van der Ark. A least squares algorithm for a mixture model for compositional data. *Computational Statistics & Data Analysis*, 30(4):359–379, 1999.
- [26] Qianqian Qi and Peter G. M. Van der Heijden. A review of NMF, PLSA, LBA, EMA, and LCA with a focus on the identifiability issue. *arXiv preprint arXiv: 2512.22282*, 2025.
- [27] Chia-Hsiang Lin, Wing-Kin Ma, Wei-Chiang Li, Chong-Yung Chi, and ArulMurugan Ambikapathi. Identifiability of the simplex volume minimization criterion for blind hyperspectral unmixing: The no-pure-pixel case. *IEEE Transactions on Geoscience and Remote Sensing*, 53(10):5530–5546, 2015.

Supplementary A: Proof of Theorem 1

The proof of Theorem 1 follows arguments similar to those in [6, 7, 9] and proceeds as follows.

Step 1: Assume that both (\tilde{M}, \tilde{H}) and $(M_{\#}, H_{\#})$ are optimal solutions for (3). Since

$$\text{rank}(\tilde{M}) = \text{rank}(\tilde{H}) = \text{rank}(M_{\#}) = \text{rank}(H_{\#}) = K,$$

there exists a full rank matrix $S \in \mathfrak{R}_+^{K \times K}$ such that

$$M_{\#} = \tilde{M}S \text{ and } H_{\#} = S^{-1}\tilde{H}.$$

Moreover, S^{-1} satisfies the column-sum-to-1 constraint since

$$\mathbf{1}^T S^{-1} = \mathbf{1}^T H_{\#} \tilde{H}^\dagger = \mathbf{1}^T \tilde{H}^\dagger = (\mathbf{1}^T \tilde{H}) \tilde{H}^\dagger = \mathbf{1}^T,$$

where \tilde{H}^\dagger denotes a right inverse of \tilde{H} , i.e., $\tilde{H} \tilde{H}^\dagger = I_K$; this inverse exists since $\text{rank}(\tilde{H}) = K$. Consequently,

$$\mathbf{1}^T S = \mathbf{1}^T \tag{1}$$

Step 2: From $M_{\#} = \tilde{M}S$, each column of S belongs to the dual cone of \tilde{M}^T , i.e.,

$$S(:, k) \in \text{cone}^*(\tilde{M}^T), \quad k = 1, \dots, K.$$

By SSC1 ($\mathbb{C} \subseteq \text{cone}(\tilde{M}^T)$), it follows that $\text{cone}^*(\tilde{M}^T) \subseteq \mathbb{C}^*$. Hence, $S(:, k) \in \mathbb{C}^*$. Therefore,

$$\|S(:, k)\|_2 \leq \mathbf{1}^T S(:, k), \quad k = 1, \dots, K. \tag{2}$$

Consequently,

$$|\det(\mathbf{S})| \leq \prod_k \|\mathbf{S}(:, k)\|_2 \leq \prod_k \mathbf{1}^T \mathbf{S}(:, k) = 1.$$

where the first inequality follows from Hadamard's inequality, the second from (2), the last equality from (1).

Step 3: If $|\det(\mathbf{S})| < 1$, then

$$\begin{aligned} \det(\mathbf{M}_\#^T \mathbf{M}_\#) &= \det(\mathbf{S}^T \tilde{\mathbf{M}}^T \tilde{\mathbf{M}} \mathbf{S}) \\ &= |\det(\mathbf{S})|^2 \det(\tilde{\mathbf{M}}^T \tilde{\mathbf{M}}) \\ &< \det(\tilde{\mathbf{M}}^T \tilde{\mathbf{M}}). \end{aligned}$$

which contradicts the optimality of $(\mathbf{M}_\#, \mathbf{H}_\#)$ for the maximum-volume criteria.

Step 4: If $|\det(\mathbf{S})| = 1$, then all the above inequalities must hold with equality. Hence,

$$\|\mathbf{S}(:, k)\|_2 = \mathbf{1}^T \mathbf{S}(:, k), \quad k = 1, \dots, K,$$

which implies that $\mathbf{S}(:, k)$ lies on the boundary of \mathbb{C}^* . Together with $\mathbf{S}(:, k) \in \text{cone}^*(\tilde{\mathbf{M}}^T)$ and SSC2, this yields

$$\mathbf{S}(:, k) = \alpha_k \mathbf{e}_k.$$

Step 5: From the constraint $\mathbf{1}^T \mathbf{S} = \mathbf{1}^T$ in Equation (1), it follows that $\alpha_k = 1$ for all k . Therefore, \mathbf{S} must be a permutation matrix.

As in minimum-volume-constrained NMF, the constraint $\mathbf{H}^T \mathbf{1} = \mathbf{1}$ in (3) can be replaced by $\mathbf{H}\mathbf{1} = \mathbf{1}$ or $\mathbf{M}^T \mathbf{1} = \mathbf{1}$. The proof follows arguments similar to those developed for MVC-NMF in [6, 7, 9] and Theorem 1.

Supplementary B: Three artificial datasets

We generate data $\mathbf{X} \in \mathbb{R}_+^{9 \times 500}$ according to $\mathbf{X} = \mathbf{M}\mathbf{H}$, where the basis matrix $\mathbf{M} \in \mathbb{R}_+^{9 \times 3}$ is nonnegative and the coefficient matrix $\mathbf{H} \in \mathbb{R}_+^{3 \times 500}$ is nonnegative with each column summing to one. Specifically, the entries of submatrix formed by the first three rows of \mathbf{M} are drawn independently from a uniform distribution between 0 and one, while the submatrix formed by the remaining six rows satisfies the sufficiently scattered condition (SSC) [6, 8, 27].

We consider three data generation settings with different sampling schemes for \mathbf{H} . In the first setting, each column of \mathbf{H} is sampled from a Dirichlet distribution with parameter (2, 0.5, 0.5) and resampled until all entries are not larger than 0.75. Under this setting, one row of \mathbf{H} contains no zero entries. Geometrically, one boundary of the simplex formed by the ground truth basis vectors does not contain any data points. As shown in Fig. B.1a, the blue circles denote data points, the blue plus signs indicate the ground truth basis vectors, and the solid blue triangle represents the simplex formed by the ground truth basis vectors. Note that in the figure, we take the ground truth basis vectors $\mathbf{M}(:, 1)$, $\mathbf{M}(:, 2)$, $\mathbf{M}(:, 3)$ as standard basis vectors \mathbf{e}_1 , \mathbf{e}_2 , \mathbf{e}_3 . In the second setting, each column of \mathbf{H} is sampled from

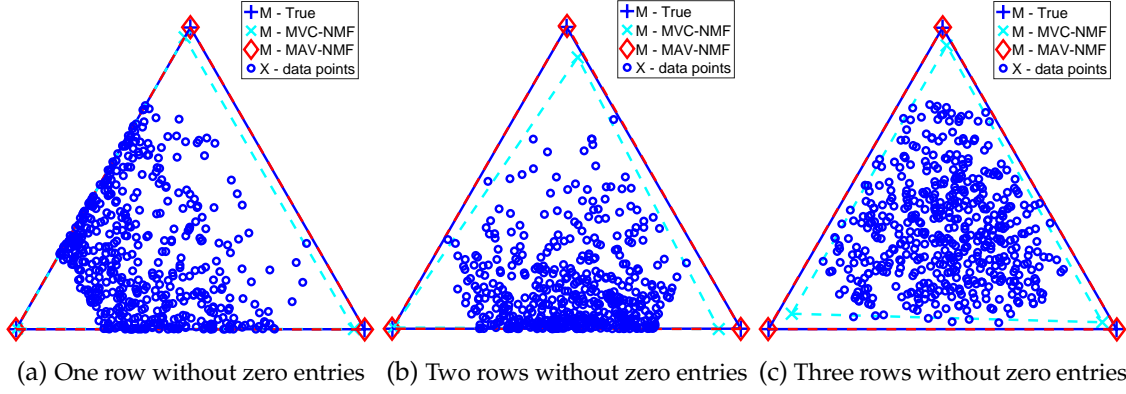


Figure B.1: Data with no zero entries in all rows of the ground truth coefficient matrix \mathbf{H} : (a) one row without zero entries; (b) two rows without zero entries; (c) all three rows without zero entries.

Table B.1: The volume of basis matrix for data where not all rows of \mathbf{H} contains zero entries; $\log\det(\mathbf{M}^T \mathbf{M} + \delta \mathbf{I})$

Methods	one row without zero entries	two rows without zero entries	three rows without zero entries
MVC-NMF	1.3720	1.1760	1.1030
MAV-NMF	1.4990	1.5040	1.5030

a Dirichlet distribution with parameter $(2, 2, 0.5)$ and resampled until all entries are not larger than 0.75, leading to two rows of \mathbf{H} without zero entries; see Figure B.1b. In the third setting, each column of \mathbf{H} is sampled from a Dirichlet distribution with parameter $(2, 2, 2)$ and resampled until all entries are not larger than 0.75, so that none of the rows of \mathbf{H} contains zero entries; see Figure B.1c.

We apply minimum-volume-constrained NMF (MVC-NMF) and maximum-volume-constrained NMF (MAV-NMF) to the artificial data \mathbf{X} to recover \mathbf{M} and \mathbf{H} . Fig. B.1a, Fig. B.1b, and Fig. B.1c show the results for the first, second, and third settings, respectively. In the figures, the cyan crosses and dashed cyan triangle correspond to the estimates obtained by MVC-NMF and the red diamonds and dashed red triangle correspond to MAV-NMF. We observe that MVC-NMF fails to recover the ground truth basis vectors, as MVC-NMF favors simplices with minimum volume, whereas the simplex formed by the ground truth basis vectors has a larger volume in these settings. In contrast, MAV-NMF achieves accurate recovery, since it can effectively expand the volume of the simplex.

Table B.1 reports the volume of the basis matrix, measured by $\log\det(\mathbf{M}^T \mathbf{M} + \delta \mathbf{I})$. We observe that MAV-NMF has larger volume than MVC-NMF. For example, for data where only one edge of the simplex has data points (the third column in Table B.1), the volumes for MVC-NMF and MAV-NMF are 1.1760 and 1.5040, respectively.

Supplementary C: Social science: Time allocation dataset

Table C.1: Time-allocation dataset [25, 26].

Activities	Male												Female																	
	12-24			25-34			35-49			50-64			65+			12-24			25-34			35-49			50-64			65+		
	1975	1980	1985	1975	1980	1985	1975	1980	1985	1975	1980	1985	1975	1980	1985	1975	1980	1985	1975	1980	1985	1975	1980	1985	1975	1980	1985	1975	1980	1985
paidwork	901	769	707	2180	1992	1899	1901	2008	2093	1708	1357	1206	176	71	95	723	665	564	439	471	704	299	375	412	151	153	233	11	6	19
dom.work	87	157	155	250	269	341	249	289	331	244	337	450	617	563	636	494	460	397	1342	1338	1147	1567	1605	1529	1600	1558	1487	1319	1409	1318
caring	33	28	15	194	206	184	99	128	136	51	54	25	124	27	38	135	99	86	635	673	651	296	309	308	83	84	82	78	154	44
shopping	120	138	127	152	157	183	173	157	185	227	221	230	273	251	264	208	200	223	347	336	336	372	347	373	376	335	352	384	292	320
per.need	289	294	316	293	316	302	351	339	332	350	364	352	365	392	383	359	377	387	311	339	337	325	346	351	367	368	385	372	453	366
eating	508	528	527	623	649	605	660	709	650	709	744	686	763	767	707	536	513	495	593	607	572	664	633	656	601	613	595	635	665	615
sleeping	3737	3765	3744	3380	3403	3397	3463	3445	3347	3560	3569	3533	3801	3871	3694	3744	3777	3821	3526	3532	3447	3567	3554	3444	3673	3701	3566	3849	3713	3675
educat.	1447	1455	1537	124	245	208	56	90	85	18	58	46	10	43	54	1163	1321	1436	77	115	120	104	98	68	27	30	40	6	21	23
particip	128	101	92	129	126	143	195	156	148	122	207	272	159	192	214	125	88	80	85	115	115	133	143	196	195	179	195	108	124	139
soc.cont	515	505	449	609	649	599	671	593	479	603	704	554	811	671	619	592	557	527	780	776	736	694	689	699	758	810	721	929	796	749
goingout	490	396	441	382	321	391	360	240	336	237	279	264	213	220	274	364	400	396	316	270	303	225	229	277	255	212	268	219	187	202
sports	419	436	485	269	279	271	206	280	291	209	299	316	297	403	476	348	370	352	306	352	368	335	440	453	323	504	545	297	482	579
gardening	111	102	100	173	213	231	259	238	268	256	288	309	366	312	308	90	76	86	149	131	145	198	154	170	197	190	217	169	191	169
outside	48	41	64	69	35	67	88	45	64	116	76	112	86	117	178	32	32	41	41	32	44	37	34	45	53	41	76	37	39	52
tv-radio	752	815	860	700	671	812	785	804	812	921	862	1012	1161	1198	1233	594	581	702	547	497	565	622	576	582	710	644	708	888	860	1076
reading	272	256	188	366	318	243	316	343	319	468	413	467	477	660	578	292	257	207	300	275	265	356	311	307	478	390	377	485	404	460
relaxing	78	56	73	64	58	57	59	44	58	79	57	68	157	92	104	73	74	63	88	54	63	76	63	59	78	53	64	63	67	69
other	146	240	200	124	172	148	188	170	146	203	190	174	223	230	225	208	234	214	199	167	164	207	174	153	212	170	230	216	204	204